# An all-digital spike-based ultra-low-power IR-UWB dynamic average threshold crossing scheme for muscle force wireless transmission

# An All-Digital Spike-based Ultra-Low-Power IR-UWB Dynamic Average Threshold Crossing Scheme for Muscle Force Wireless Transmission

{Amirhossein, Masoud} Shahshahani[1], Paolo Motto Ros[2], Alberto Bonanno[2],
Marco Crepaldi[2], Member IEEE, Maurizio Martina[1], Member IEEE,
Danilo Demarchi[1,2], Senior Member IEEE, Guido Masera[1], Senior Member IEEE.
Politecnico di Torino – Department of Electronics and Telecommunications (DET)[1], Istituto Italiano di Tecnologia@PoliTo[2]
Email: guido.masera@polito.it, danilo.demarchi@iit.it

***Abstract*—We introduce an Impulse Radio Ultra-Wide Band (IR-UWB) radio transmission scheme for miniaturized biomedical applications based on a dynamic and adaptive voltage thresholding of surface Electro Myo Graphy (sEMG) signals. The amplified sEMG signal is compared to a DAC-generated threshold computed from the previous 1-bit history by custom digital control logic running at 2kHz clock and implementing an ad-hoc algorithm (Dynamic Average Threshold Crossing, D-ATC). The resulting events and the associated digitized voltage level can be both asynchronously radiated through IR-UWB. Analyzes show that the scheme is robust w.r.t. the sEMG signal variability and correlates by ∼96% with regard to raw muscle force information after signal is recomputed at the RX. This paper compares D-ATC with regard to a fixed threshold system and an Average Threshold Crossing (ATC) demonstrating improved robustness, and introduces the thresholding algorithm verified on a dataset of 190 sEMG recorded signals. The applied threshold resolution has been optimized to both minimize the size of transmitted data and to guarantee good correlation performance. The paper concludes with post-synthesis results of the D-ATC compact digital control logic in a 0.18$\mu$m CMOS process, demonstrating an extremely low power consumption at very low active area expenses.**

## I. Introduction

Impulse-Radio Ultra-Wide Band (IR-UWB) technology is at present well known and widely used in experimental in Wireless Body Area Networks (WBAN) and miniaturized biomedical applications [1], [2] thanks to its inherent aggressive duty cycling, its low energy per bit and the enabling of low form factor antennas [3]. IR-UWB is a wireless technology strongly tied to the concept of time, where very short duration (nanosecond duration order) pulses [4], [5] are radiated following precise temporal relationships, normally exploiting Pulse-Position Modulation (PPM) or On-Off-Keying (OOK) [6], but asynchronous communication paradigms are also possible [7], provided that pulses Power Spectral Density (PSD) level does not exceed the -41.3 dBm / MHz limit [4]. For instance, recent applications exploit sEMG signals for hand-exoskeleton control, where bioreceptors data are directly used for actuation purposes and human-machine interactions [8]. In this context, the transmission of the sEMG signal, i.e. (ADC conversion), impacts on the area and power consumption of the TX.

In [9] the application of raw thresholding on the sEMG signals for the wireless transmission of force information over-the-air have been demonstrated. Average Threshold Crossing (ATC) has been defined as the asynchronous radiation of a UWB pulse every time the sEMG signal overcomes a threshold. The average number of radiated pulses is demonstrated to be proportional to the applied muscle force and at the receiver a low-complexity windowing can be applied to recover the transmitted force information. However, from a system-level point of view, notwithstanding its promising features in terms of noise robustness, ATC needs a threshold setting to generate pulse events to be transmitted. From a system-level point of view, the use of a fixed threshold implies gain controllability at the sEMG preamplification stages so that signal dynamic range can be adapted and matched to the required threshold-level. From another complementary viewpoint, the same issue can imply a threshold-level adjustment to adapt the gain variations of the sEMG preamplifier which may vary based on the electrodes-skin interface. In any case, the application of a hard decision mechanism on an analog signal (i.e., single thresholding '0' or '1', *all-or-none*) requires careful control of its features to operate without additional calibration mechanisms.

The system introduced in this work (Fig. 1), and detailed in Sec. III, is based on simply triggering a wireless pattern event every time the sEMG signal crosses a threshold dynamically computed on incoming events resulting from an EMG signal thresholding (Fig 2), Dynamic Average Threshold Crossing (D-ATC). With the proposed scheme, the same low-complexity radio transceiver chipset in [10] can be used to wirelessly

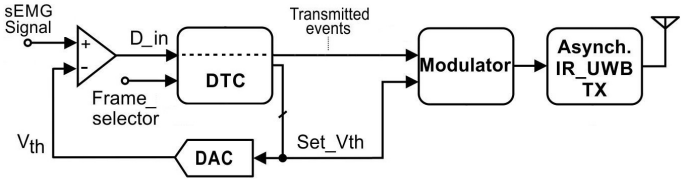


Fig. 1. Dynamic Average Threshold Crossing (D-ATC) transmitter block diagram.

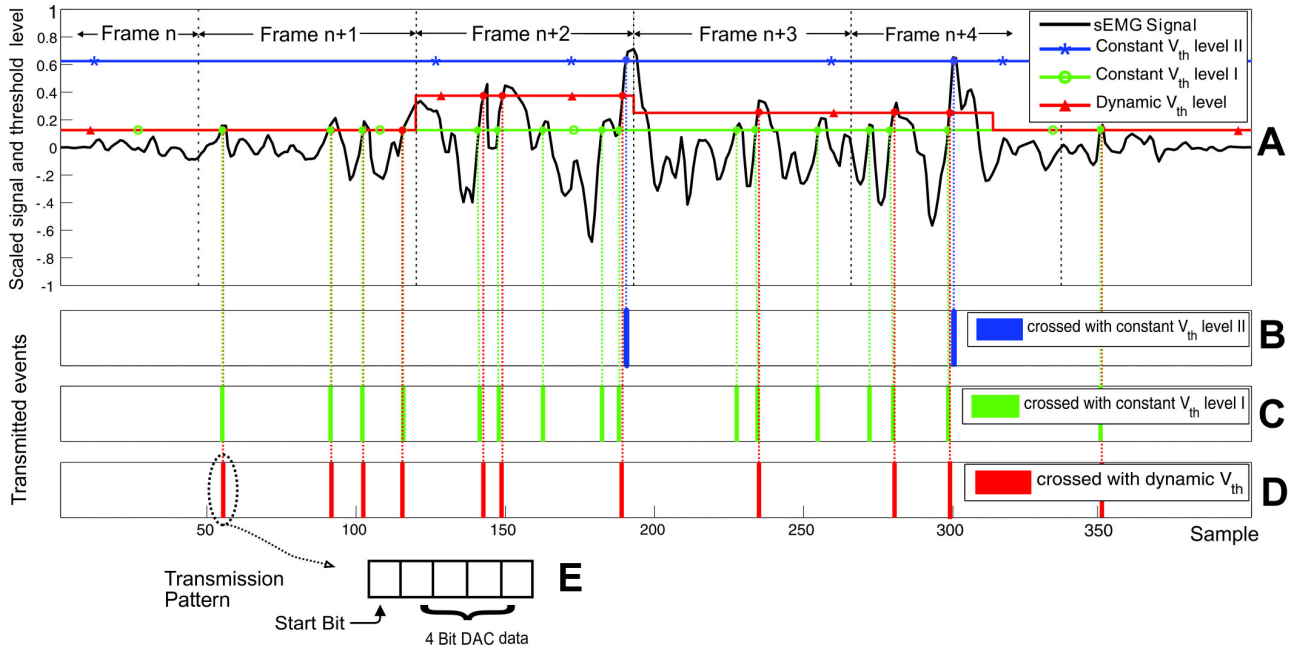


Fig. 2. Comparison between dynamic and constant thresholding techniques: A) a simple sEMG signal divided into frames, B, C) transmitted events for constant $V_{\text{th}}$ approach (ATC) in two different voltage threshold levels, D) transmitted events for the new proposed dynamic algorithm (D-ATC), E) a representation of the transmitted data packet used in the D-ATC every time an event is issued.

transmit a muscle force signal (see Sec. II and III): the sEMG signal can thresholded and the digital positive-edge crossing events can be asynchronously transmitted and received by the RF-CMOS IR-UWB radio in [7] and [11], using an Address-Event Representation (AER) signaling protocol as proposed in [12].

A laptop can collect events in the receiver (RX) and perform the required biomedical analyzes. Using a set of biomedical sEMG data collected on several different subjects, we demonstrate in Sec. III part B that our D-ATC scheme features high correlation to real muscle force signal compared to the constant thresholding. Moreover, hardware architecture, simulation and post-synthesis results are depicted in Sec. III part C to demonstrate the low cost and low power feasibility of our approach according to its high efficiency.

## II. Dynamic Average Threshold Crossing

The event transmission with an ATC implies the comparison of the sEMG signal with a fixed threshold $V_{\text{th}}$ that is, as represented in Fig. 2(B) and (C). The depicted plots are useful to have a clear view of the advantages of a dynamic threshold compared to a constant threshold. In (A) a simple sEMG signal is divided into frames, in (B) and (C) transmitted events are generated with a constant $V_{\text{th}}$ (ATC) with two different thresholds, in (D) transmitted events are generated by the proposed dynamic algorithm and in (E) a representation of the transmitted data pattern used in D-ATC, issued by the RF modulator every time an event is generated. To transmit the sEMG signal with a wireless transceiver, a standard system would require an A-to-D converter and communication would be packet-based. Typically additional bits, e.g. header, Start-Frame-Delimiter (SFD), identifier (ID) and Cyclic Redundancy Code (CRC) are required for a transmission packet as supplementary symbols. To transfer each sample, considering as an example an 8-bits A/D converter, in general a packer including an 8 bit payload is needed. Generally, the extra symbols required by the packet-based commnunication also depend on the number of users and in general also to the protocol.

ATC joined to asynchronous IR-UWB permits power consumption decrease at the TX, since the transmission of an event occurs at a non-fixed pulse rate and it is data dependent. As shown in Fig. 2, in ATC [10] an UWB transmission event is generated when the amplified sEMG signal crosses $V_{\text{th}}$: the wireless system transmits at about 1 kbps in the worst case of sEMG signal at 1 kHz, but it is very unlikely that the system constantly fires at such rate. However, since the signal is compared with a fixed threshold voltage, low amplitude signals below $V_{\text{th}}$ can not be sensed by the comparator [see Fig. 2(B)]. On the contrary, considering a case in which the $V_{\text{th}}$ level is lower than the average sEMG signal amplitude, a large number of events are generated. As a consequence, the number of transmitted events increases, therefore the power consumption at the TX. The algorithm proposed in this work is based on the dynamic control of the $V_{\text{th}}$ to track the mean sEMG signal level, hence keep the firing rate controlled while maintaining at the same time a low number of transmitted symbols compared to packet-based communication. For this purpose, we split the signal into contiguous frames. The Dynamic Threshold Controller (DTC) block predicts the $V_{\text{th}}$ level of next frame

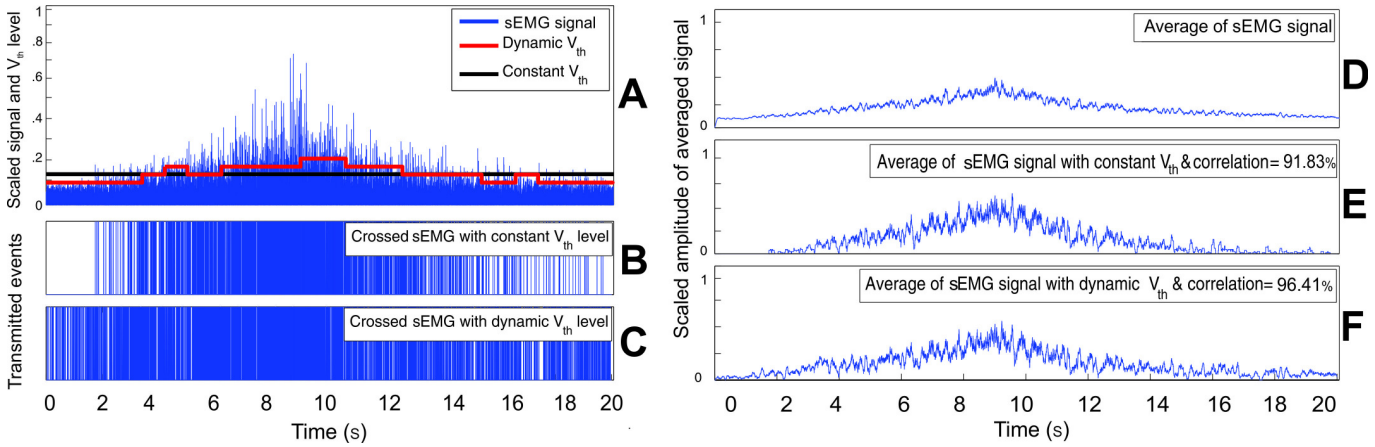


Fig. 3. Comparison between constant ($V_{\text{th}}$=0.3 V) and dynamic thresholding for a real sEMG signal with 50000 samples, 20 seconds: A) rectified sEMG signal with constant and dynamic $V_{\text{th}}$ levels, B, C) transmitted events generated by crossing sEMG signals with constant and dynamic thresholds, E, F) the reconstructed sEMG signals correlations with respect to the original (D).

based on the number of events that have been detected during the previous frames (see Fig. 2). As a consequence, we have almost the same number of events for both low and high sEMG signal level.

A Dynamic Threshold Controller (DTC) together with a simple Digital to Analog converter (DAC) have been added to the basic ATC [10] scheme so that they can operate as a voltage threshold trimmer (see Fig. 1). Different DAC resolution have been examined to determine the best trade-off between accuracy and complexity, considering the threshold level and the minimization of the transmission data packet length.

Fig. 3 compares a constant [10] with the proposed dynamic average threshold crossing algorithm for a real sEMG signal. As it can be observed, ATC can not sense low voltage levels of the sEMG signal. It is worth noting that, people with different skin thickness and gender have dissimilar sEMG voltage levels, hence, according to the input signal level, the fixed threshold voltage can not be adopted but it has to be trimmed on a case by case basis. On the contrary, the proposed solution which is very flexible, has been designed both to match and adapt the threshold voltage to the input signal for a significant number of cases. The average rectified value of the sEMG signals is acquired at the receiver as shown in Fig. 3(E) and (F). All sEMG signal voltage levels are sensed with a correlation rate of 96.41% [Fig. 3(F)], which is almost 5% higher with respect to constant thresholding [Fig. 3(E)].

## III. Dynamic Threshold Controller Architecture

### A. Implementation

The input of the DTC is an amplified sEMG signal which is connected to the analog comparator as shown in Fig. 1. This input signal is compared with a voltage threshold generated by a DAC `Set_Vth` to dynamically control "firing rate". The output of the DTC is in turn `D_in`, now resampled hence synchronized with the DTC system clock, to be processed by the next modulator. The 4-bit DAC used in this work creates a voltage threshold $V_{\text{th}}$ that varies from 0 to 1 V with 16 steps, accurate enough for this application. The DTC uses the one bit signal `D_in` to examine the mean time when sEMG signal is higher than $V_{\text{th}}$. For this purpose, at each clock cycle the counter in the DTC architecture (Fig. 4) is increased when `D_in`='1'. The block adjusts the $V_{\text{th}}$ level by monitoring the number of ones and zeros of `D_in` during a frame. The frame length is programmable (`Frame_selector` signal) and can be 100, 200, 400 or 800 times the system clock period. In order to have an adaptive voltage threshold, it is required to implement a feedback from the previous frames data. Trading-off complexity and accuracy, three last frames are selected to count the number of ones (named as `N_one_i`). The algorithm is based on the weighted average (Eqn. (1)) of the number of ones in the last three frames. Data elements with a high weight contribute more to the weighted mean than do elements with a low weight. In our case, $W_{F3} = 1, W_{F2} = 0.65, W_{F1} = 0.35$ are considered based on data acquired through real experiments. The weighted average $\bar{x}$ is defined as:

$$\bar{x} = \frac{\sum_{i=1}^{n} w_i x_i}{\sum_{i=1}^{n} w_i}, \tag{1}$$

where $w_i$ and $x_i$, represent weight and quantity.

The quantity is compared with interval numbers (referred to `interval_level_i` in the algorithm, see Lst. 1) which are generated internally depending on the selected frame size. These intervals are computed as in Eqn. (2). If the frame reaches the end, `N_one_i` data shift to the `N_one_(i-1)` and the *Predictor* block generates a new $V_{\text{th}}$ level (named `Set_Vth`) based on the average computed at the end of current frame and the selected frame size at the input. The `End_of_frame` signal acts as a flag to represents start or end of frames. Finally, the transmitter sends the digital sEMG signal, `D_out`, together with the $V_{\text{th}}$ level and any other required data. Steps are summarized in Lst. 1. `N_one`$i$ identifies the number of '1' counted in an $i$-th frame (overall 3), and `AVR` is the weighted average defined in Eqn. (1).

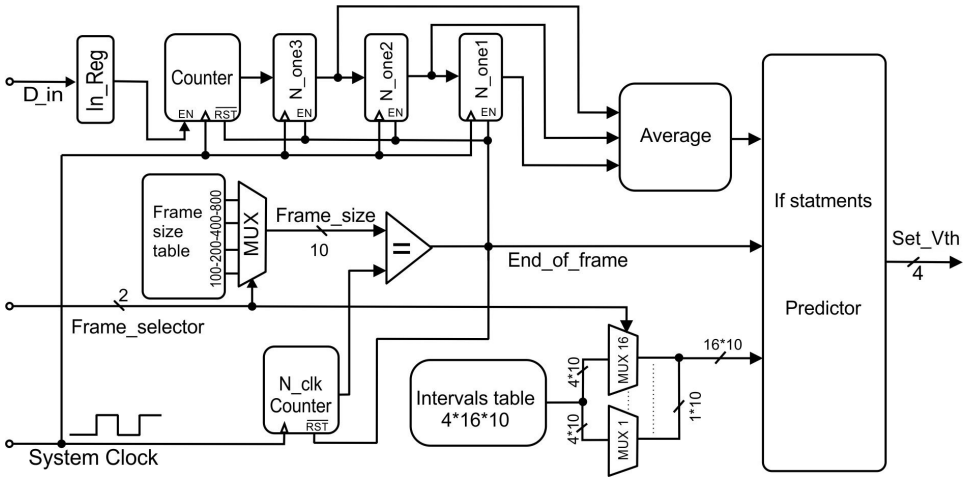


Fig. 4. Detailed block scheme of the Dynamic Threshold Controller (DTC) with details on each internal sub-system.

Listing 1. D-ATC algorithm.

```
if End_of_frame then

  AVR= ((W_F3*N_one3 + W_F2*N_one2
         + W_F1*N_one1)/2);

  if AVR >= interval_level_15 then
      set_Vth = 15;
    elsif AVR >= interval_level_14 then
      set_Vth = 14;
    .
    .
    .
    elsif AVR >= interval_level_2 then
      set_Vth = 2;
    else
      set_Vth = 1;
  end

  N_one1 = N_one2;
  N_one2 = N_one3;

end
```

The quantities `interval_level_`$i$ are computed as follows:

$$\begin{aligned}
&\texttt{interval_level_15} = 0.48 \times \texttt{frame_size};\\
&\texttt{interval_level_14} = 0.45 \times \texttt{frame_size};\\
&\qquad\qquad\qquad\qquad\vdots\\
&\texttt{interval_level_1} = 0.06 \times \texttt{frame_size};\\
&\texttt{interval_level_0} = 0.03 \times \texttt{frame_size}.
\end{aligned} \tag{2}$$

The design has been optimized to reduce the computation time and also the component silicon area. In particular, see Eqn. (2), instead of multiplying constant numbers (i.e, 0.48, 0.45, 0.06 and so on) to the `frame_size` we considered a look-up table which stores the precalculated results of the products of Eqn. (2) with all possible `frame_size` to save area and computation time.

The algorithm constants and parameters have been determined empirically based on a very large set of data. The maximum frame length is 800, therefore 10 bit are enough for the `frame_size` signal vector. Consequently, 10 bit signals are considered for wiring all counters, shift registers and multiplexers. The look-up `Intervals table` includes the overall 16 intervals computed as in Eqn. (2), to identify all the 16 possible DAC levels, for all frame lengths, i.e., `interval_level_(0:15) = interval_table(Frame_selector)`.

When the EMG signal amplitude changes within the algorithm windowing time, the number of ones at each frame changes and, as a result, the average of last three frames. Consequently, the $V_{\text{th}}$ level is increased or decreased. The analog threshold applied to the comparator is generated by the D-to-A converter, based on the simple Eqn. (3):

$$V_{\text{th}} = (V_{\text{ref}} \times \texttt{Set\_Vth})/(2^{N_b}), \tag{3}$$

where $V_{\text{ref}}$ is the reference voltage of the DAC, which is here assumed 1 V, and $N_b$ is the number of bits, here, 4.

### *B. Simulations with Measured EMG Signals*

To examine the overall algorithm performance compared to the basic ATC, we have considered the same 190 patterns used for fixed thresholding. Each pattern contain 50000 samples for 20 seconds muscle activity. The data samples refer to eight healthy male ($30 \pm 2$ years old) with 70% of their Maximum Voluntary Contraction (MVC) to 0% using a cylindrical power grip are acquired [10]. One second is the duration of MVC sustained with maximum contraction of which the mean value is taken. Along the phase three differential electrodes are placed on the ventral region of the forearm muscles and 1000 k samples/s sEMG signals are acquired using a Biometrics DataLINK system. Simulation results for these sEMG signal data assert to the reality of the proposed adaptive algorithm by calculating correlations are shown in Fig. 5. In this figure, the

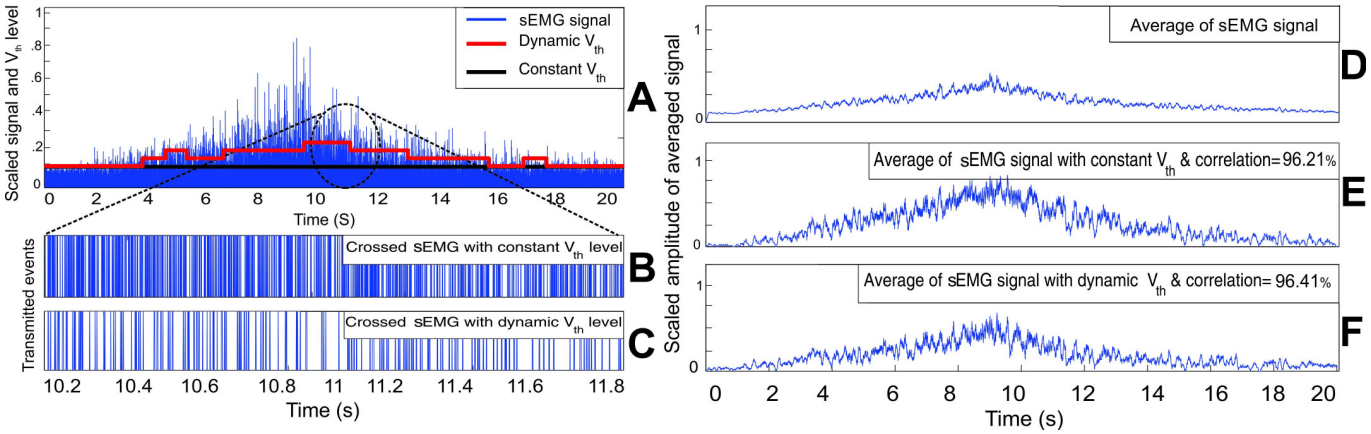


Fig. 6. A comparison between the percentage of correlation and transmitted events for constant and dynamic thresholding of a real sEMG signal, 50000 samples, 20 seconds, with zoom-in. Compared to Fig. 3, here the voltage threshold used is $V_{\text{th}} = 0.2$ V.

correlation percentage for constant thresholding varies from 47% to 95.2% while for D-ATC, lower fluctuation is present and the variation is between 85% to 98%. Signals with lower amplitude compared to the constant $V_{\text{th}}$ witness the minimum percentage of correlations. Even if we add some pulses due to the artifacts we believe that the signal is still received with a good correlation, as artifacts effect is similar to pulse missing.

The dynamic thresholding technique is even stable as a function of the number of transmitted events for different patterns while in the constant thresholding it is not. Matlab simulations show that the number of transmitted events for dynamic thresholding (see Fig. 3) with higher correlation is 3724 which is almost 17% more than constant ATC, with 3183 pulses, assuming the same sEMG signal samples. Fig. 6 uses the same sEMG signal as in Fig. 3, used as input but with lower threshold level of $V_{\text{th}}$=0.2 V, so that we can increase the correlation of sEMG signal with the until we reach those of D-ATC. By specifically looking at the zoomed area in Fig. 3, the number of transmitted events in ATC is higher than in D-ATC, with 5821 events that is almost 56% more than D-ATC. In other words, by choosing the same signal as input, in both Fig. 3(F) and Fig. 6(F) the correlation is the same, while in Fig. 3(E) and Fig. 6(E) we have correlation mismatch due to the different threshold level $V_{\text{th}}$.

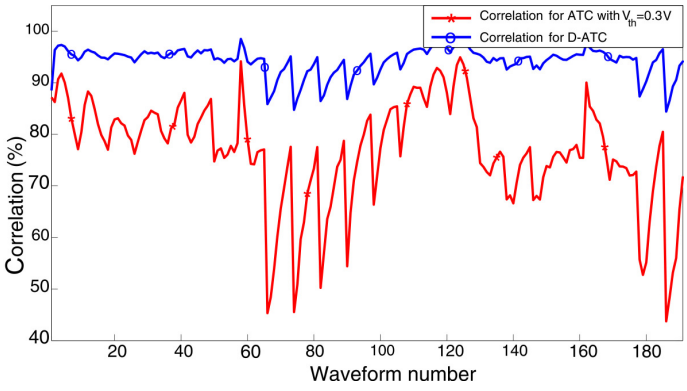


Fig. 5. Comparison between D-ATC and ATC ($V_{\text{th}}$=0.3 V), correlation results for 190 patterns.

Considering a standard packet and ADC-based wireless transmission, together with the required complementary bits to provide physical and data synchronization (header), a very large number of pulses should be transmitted. On the other hand, for ATC and D-ATC a pattern-based communication holds: the same sEMG signal is considered but with different voltage levels for constant threshold as in Fig. 3 and Fig. 6. We report an example number of transmitted pulses for a single EMG wave data lasting 20 s, assuming for all cases an IR-UWB link (12 bit ADC data for standard systems),

- Standard packet-based system – $12 \times 50000 = 600000$ symbols;
- ATC system ($V_{\text{th}}$=0.3 V) – $3183 \times 1 = 3183$ event symbols;
- ATC system ($V_{\text{th}}$=0.2 V) – $5821 \times 1 = 5821$ event symbols;
- D-ATC system – $3724 \times 5 = 18620$ event symbols.

We conclude that D-ATC increases a the number of pulses while providing significant advantages compared to ATC, but still maintaining a number of transmitted symbols very low compared to a packet-based communication.

Fig. 7 comprises other quantitative results and makes comparison between the number transmitted events and their correlations at different $V_{\text{th}}$ levels. Four different sEMG signals are randomly selected from previous 190 patterns. It is clear that D-ATC is more stable from the transmitted events viewpoint and maintains performance figures close to the real sEMG signal compared to the fixed threshold ATC, using two different $V_{\text{th}}$ levels.

### C. Hardware Implementation

To determine the physical impact of the DTC, we implemented the architecture using a Hardware Description Language (HDL) and synthesized the description using a digital standard cell library in a high voltage 0.18$\mu$m CMOS technology. The description is simulated and synthesized in Modelsim and Synopsis, respectively. The post synthesis Verilog netlist

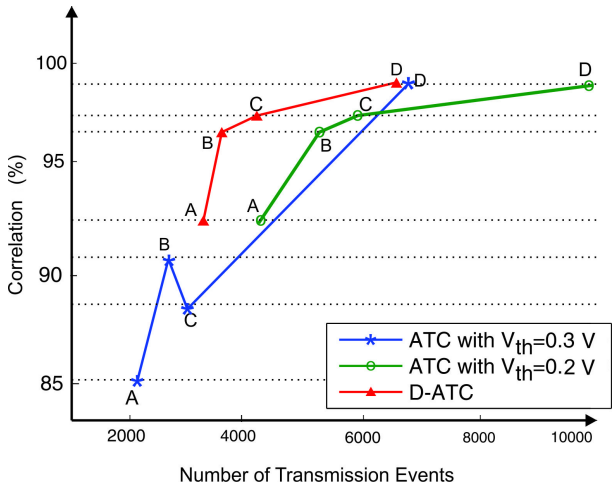


Fig. 7. Trade-off between transmitted events and the correlation level w.r.t. raw muscle force in ATC and D-ATC. Point B is discussed as an example in Sec. II B.

together with timing constraint files are again used to check timing analysis and dynamic power consumption of the DTC architecture. We have verified that Verilog results perfectly match the Matlab simulation outputs.

For lossless digitization, the sampling rate should be at least twice the maximum frequency response of input signal (sEMG) w.r.t the Nyquist sampling theory. $f_{clk} = 2f_{sEMG}$, where $f_{clk}$ is the system clock and $f_{sEMG}$ is the maximum frequency of the EMG signal. $f_{sEMG}$ is about 1 kHz, and $f_{clk}$ is set to the maximum of 2 kHz so that to demonstrate both the sampling rate and the minimum dynamic switching activity. Since the input signal is not synchronous, and metastability can occur whether an asynchronous event is sampled by the DTC, an internal register `In_reg` is placed to make data-flow synchronous with clock. Moreover, a two bit additional selection input is considered to enable a user to choose the possible 4 `frame_size`. The overall input signals are `D_in` and `system clock`, a 4-bit signal vector `Set_Vth`. The block comprises other 8 bit outputs (for ADC and internal states). The IP comprises an asynchronous reset signal `RST`, a system enable signal `EN` and the power supply pins `VDD` and `GND`. Simulation and synthesis results are summarized in table I.

TABLE I
SIMULATION AND SYNTHESIS RESULTS.

| | |
|---|---|
| Power supply | 1.8 V |
| System clock frequency | 2 kHz |
| Number of cells | 512 |
| Number of ports | 12 |
| Core area | 11700 $\mu$m$^2$ |
| Dynamic power consumption | ~70 nW |

## IV. CONCLUSION

We introduced an all-digital spike-based muscle force IR-UWB wireless system based on Dynamic Average Threshold Crossing (D-ATC) events. With its low hardware complexity and low power dissipation, D-ATC provides high signal correlation w.r.t. to applied muscle force, higher w.r.t. to a fixed thresholding (ATC). Measurements and analysis on 190 recorded sEMG signals show very good correlation maintaining extremely low active area and power consumption when the system is implemented in a high voltage 0.18$\mu$m CMOS technology.

## REFERENCES


[1] M. R. Yuce, "Implementation of Wireless Body Area Networks for Healthcare Systems," *Sensors and Actuators A: Physical*, vol. 162, no. 1, pp. 116–129, Jul. 2010.

[2] B. Latré, B. Braem, I. Moerman, C. Blondia, and P. Demeester, "A Survey on Wireless Body Area Networks," *Wireless Networks*, vol. 17, no. 1, pp. 1–18, Jan. 2011.

[3] M. R. Yuce, T. S.P. Seeb, and C. K. Hoa, "An Ultra-Wideband Wireless Body Area Network: Evaluation in Static and Dynamic Channel Conditions," *Sensors and Actuators A: Physical*, vol. 180, pp. 137–147, Jun. 2012.

[4] Federal Communications Commission (FCC), "Revision of Part 15 of the Commissions Rules Regarding Ultra-Wideband Transmission Systems, First Report and Order," *Feb.*, 2002.

[5] A. F. Molisch, K. Balakrishnan, D. Cassioli, C.-C. Chong, S. Emami, A. Fort, J. Karedal, J. Kunisch, H. Schantz, U. Schuster, *et al.*, "Ieee 802.15. 4a channel model–final report," 2004.

[6] Y. Gao, S. Diao, C.-W. Ang, Y. Zheng, and X. Yuan, "Low Power Ultra-wideband Wireless Telemetry System for Capsule Endoscopy Application," in *IEEE Conference on Robotics Automation and Mechatronics*, Jun. 2010, pp. 96–99.

[7] Crepaldi, M. and Demarchi, D. and Civera, P., "A Low-complexity Short-distance IR-UWB Transceiver for Real-time Asynchronous Ranging," in *Fly by Wireless Workshop (FBW)*, Jun. 2011, pp. 1–4.

[8] W. Ryu, B. Han, and J. Kim, "Continuous Position Control of 1 DOF Manipulator Using EMG Signals," in *International Conference on Convergence and Hybrid Information Technology*, vol. 1, Nov. 2008, pp. 870–874.

[9] P. Ros, M. Paleari, N. Celadon, A. Sanginario, A. Bonanno, M. Crepaldi, P. Ariano, and D. Demarchi, "A Wireless Address-event Representation System for ATC-based Multi-channel Force Wireless Transmission," in *IEEE International Workshop on Advances in Sensors and Interfaces (IWASI)*, Jun. 2013, pp. 51–56.

[10] M. Crepaldi, M. Paleari, A. Bonanno, A. Sanginario, P. Ariano, D. Tran, and D. Demarchi, "A Quasi-digital Radio System for Muscle Force Transmission Based on Event-driven IR-UWB," in *Biomedical Circuits and Systems Conference (BioCAS)*, Nov 2012, pp. 116–119.

[11] M. Crepaldi, D. Dapra, A. Bonanno, I. Aulika, D. Demarchi, and P. Civera, "A Very Low-Complexity 0.3–4.4GHz 0.004mm$^2$ All-Digital Ultra-Wide-Band Pulsed Transmitter for Energy Detection Receivers," *IEEE Transactions on Circuits and Systems I: Regular Papers*, vol. 59, no. 10, pp. 2443–2455, Oct. 2012.

[12] P. Motto Ros, M. Crepaldi, A. Bonanno, and D. Demarchi, "Wireless Multi-channel Quasi-digital Tactile Sensing Glove-Based System," in *Digital System Design (DSD)*, Sept. 2013, pp. 673–680.